

DOI: 10.1002/cssc.201200680

# Nitrogen-Doped Porous Carbon Nanosheets as Low-Cost, High-Performance Anode Material for Sodium-Ion Batteries

Heng-guo Wang,<sup>[a]</sup> Zhong Wu,<sup>[a, b]</sup> Fan-lu Meng,<sup>[a, c]</sup> De-long Ma,<sup>[a, c]</sup> Xiao-lei Huang,<sup>[a, b]</sup> Li-min Wang,<sup>[a]</sup> and Xin-bo Zhang<sup>\*[a]</sup>

During the past years the successful development of lithium-ion batteries (LIBs) has led to them seizing the portable electronics market, and they are playing an ever-growing role in the field of large-scale energy storage, for example in applications for electric vehicles and renewable energy storage. The higher demands placed on LIBs as a result of this growing importance has increased concern about the high costs and the limited reserves of lithium.<sup>[1]</sup> In sharp contrast to lithium, sodium resources are beyond doubt practically inexhaustible, ubiquitous, and environmentally benign, and these factors have stimulated worldwide interest in sodium-ion batteries (NIBs) as a low-cost alternative to LIBs.<sup>[2]</sup> However, because the sodium ion is ca. 55% larger than the lithium ion, finding suitable host materials with sufficiently large interstitial space to accommodate sodium ions and to allow reversible and rapid ion insertion and extraction is very difficult. It is well-established that graphite, the dominant anode material in today's commercial LIBs, is not suitable for sodium-based systems because sodium ions hardly form staged intercalation compounds with graphite.<sup>[3]</sup> Disordered carbon appears to be the most suitable anode material for NIBs. For example, previous pioneering works have demonstrated reversible sodium ion intercalation in a variety of carbonaceous materials such as petroleum cokes,<sup>[4]</sup> carbon black,<sup>[5]</sup> carbon fiber,<sup>[6]</sup> and pyrolytic carbon.<sup>[7]</sup> Very recently, Tang et al. demonstrated the use of hollow carbon nanospheres, obtained from glucose pyrolyzed in the presence of latex templates, as superior-rate anode materials for NIBs.<sup>[2b]</sup> Later, Cao et al. reported that hollow carbon nanowires, prepared from a pyrolyzed hollow polyaniline nanowire

precursor, display a high reversible capacity of 251 mAhg<sup>-1</sup> and excellent cycling stability over 400 cycles.<sup>[2c]</sup> Although much progress has been realized, NIBs are currently still in their infancy. Great improvements are urgently needed, and suitable electrode materials are at the top of the list.

Two-dimensional carbon nanostructures, especially 2D porous carbon materials, are being increasingly researched for energy storage/conversion devices. They offer significant improvements in power and energy density compared to bulk electrodes because they enable large surface-to-volume ratios for contact with the electrolyte, continuous conducting pathways through the electrodes for electrons, and facile strain relaxation during battery operation.<sup>[8]</sup> Further, the incorporation of heteroatoms seems to be the most promising method for enhancing capacity, surface wettability, and electronic conductivity.<sup>[9]</sup> For example, the presence of nitrogen species on a carbon surface can lead to a pseudocapacitive interaction between the electrolyte ions and the nitrogen-containing functional groups.<sup>[9b]</sup> Many nitrogen-doped carbon materials have been prepared by chemical vapor deposition, thermal annealing with NH<sub>3</sub>, nitrogen plasma treatment, and the arc-discharge method.<sup>[10]</sup> However, these methods suffer from more or less-severe drawbacks, such as the requirement of toxic precursors, sophisticated equipment, special instruments, and/or rigorous conditions. Therefore, the preparation of nitrogen-doped carbon materials by a facile method is still a challenge.<sup>[9e, f]</sup> Because both strategies, that is, the use of 2D porous carbon materials and introducing heteroatoms, result in improved electrochemical performances, there is a large interest in developing carbon nanostructures that combine them. However, to the best of our knowledge, there is no report on the fabrication of 2D carbon materials, nor on the use of porous, nitrogen-doped, alkaline-activated carbon nanosheets derived from polypyrrole-functionalized graphene, for NIBs.


Herein, we describe a strategy to synthesize 2D porous nitrogen-doped carbon sheets by chemical activation of polypyrrole (PPy)-functionalized graphene sheets with KOH (ANPGs). Benefiting from the unique porous nanostructure and nitrogen doping, the ANPGs exhibit a high reversible capacity (349.7 mAhg<sup>-1</sup> at 50 mA g<sup>-1</sup>), good cycling stability over 260 cycles, and good rate capability (50 mAhg<sup>-1</sup>, even at a very high current density of 20 A g<sup>-1</sup>).

Figure 1 outlines the strategy used to synthesize the ANPGs. Firstly, thin, sandwich-like graphene oxide-polypyrrole sheets were fabricated by chemical polymerization of pyrrole on the surface of graphene oxide (GO), with the aid of ammonium

[a] Dr. H.-g. Wang, Z. Wu, F.-l. Meng, D.-l. Ma, X.-l. Huang, Prof. Dr. L.-m. Wang, Prof. Dr. X.-b. Zhang  
State Key Laboratory of Rare Earth Resource Utilization  
Changchun Institute of Applied Chemistry  
Chinese Academy of Sciences  
Changchun 130022 (PR China)  
Fax: (+86)431-8526-2247  
E-mail: xbzhang@ciac.jl.cn

[b] Z. Wu, X.-l. Huang  
University of Chinese Academy of Sciences  
Beijing 100049 (PR China)

[c] F.-l. Meng, D.-l. Ma  
Key Laboratory of Automobile Materials  
Ministry of Education  
and School of Materials Science and Engineering  
Jilin University  
Changchun 130012 (PR China)

 Supporting Information for this article is available on the WWW under <http://dx.doi.org/10.1002/cssc.201200680>.

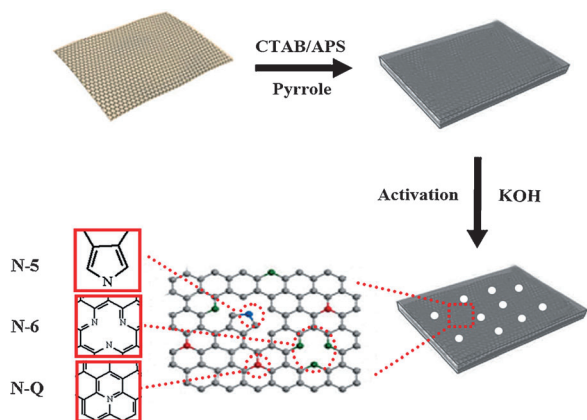


**Figure 1.** Strategy for preparing the nitrogen-doped carbon sheets (ANPGs), involving activation of polypyrrole-functionalized graphene.

persulfate. The nanosheets were subsequently chemically activated with KOH at 800 °C for 2 h under a nitrogen atmosphere,<sup>[11]</sup> resulting in porous nitrogen-doped carbon nanosheets with large surface areas. By this polymerization, carbonization, and activation process the nitrogen atoms are expected to replace the carbon atoms in the original graphene sheets, forming three types of nitrogen configurations: pyridine-like (N-6), pyrrole-like (N-5), and graphite-like (N-Q). As illustrated in Figure 1, in this manner we hope to make use of the better conductivity of heteroatom-doped carbon materials as well as the open, shortened paths offered by 2D nanostructured materials.

The morphology of the resulting ANPGs was characterized by scanning electron microscopy (SEM) and transmission electron microscopy (TEM). The ANPGs obviously maintained their 2D structure, but the surface morphology featured more corrugations compared to bare graphene, indicating the growth of polypyrrole along the surface of the graphene oxide sheets (Figure 2a, and Supporting Information Figures S1 and S2).<sup>[9a]</sup> The HRTEM image in Figure 2b shows the formation of porous

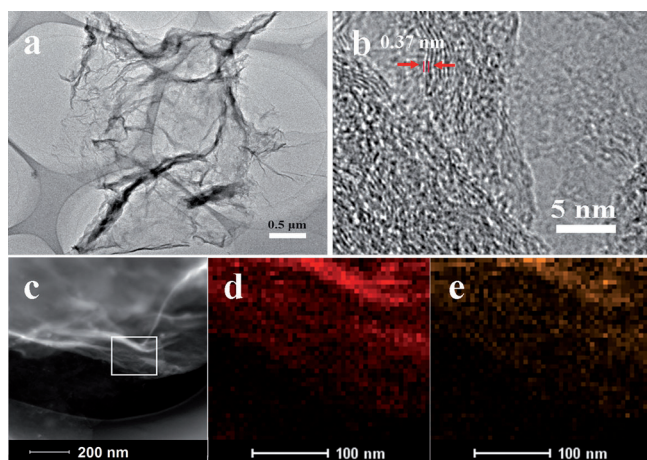


**Figure 2.** a) TEM, and (b) HRTEM image of ANPGs. c) Dark-field TEM image of ANPGs, and corresponding elemental mapping images of d) carbon and e) nitrogen.

carbon after activation with KOH, and shows that the average spacing between the graphene layers was about 0.37 nm (Figure 2b). An X-ray diffraction (XRD) measurement (Figure S3) on the ANPGs revealed two weak, broad diffraction peaks at around  $2\theta = 24.3^\circ$  and  $44.4^\circ$ . These peaks correspond to the (002) diffraction of the graphitic layer-by-layer structure and the (101) diffraction of graphite, respectively. The interlayer spacing ( $d_{002}$ ) was calculated as 0.37 nm, corroborating the HRTEM results. Notably, the interlayer spacing of 0.37 nm can be beneficial for the insertion/extraction of sodium,<sup>[2c]</sup> which is an important property for its reversible storage, considering the larger diameter of sodium ion (0.95 Å) compared to lithium ion (0.60 Å). In addition, scanning TEM (STEM) and elemental mapping analyses revealed uniform distributions of carbon (Figure 2d) and nitrogen (Figure 2e).

To further examine the surface and characterize the pore size of the ANPGs,  $N_2$  adsorption–desorption isotherms were measured. The nitrogen-doped carbon sheets exhibited type IV isotherms, with a distinct hysteresis loop at a relative pressure  $P/P_0$  ranging from 0.4 to 1, and a high Brunauer–Emmett–Teller surface area of  $1477 \text{ m}^2 \text{ g}^{-1}$  (Figure 3a; the pore size distribution is shown in the inset). The nitrogen-doped carbon sheets display a high pore volume of  $2.02 \text{ cm}^3 \text{ g}^{-1}$ , and possess both small micropores (peak at 1.41 nm) and mesopores (peaks at 2.77 and 3.79 nm), again corroborating the HRTEM results.

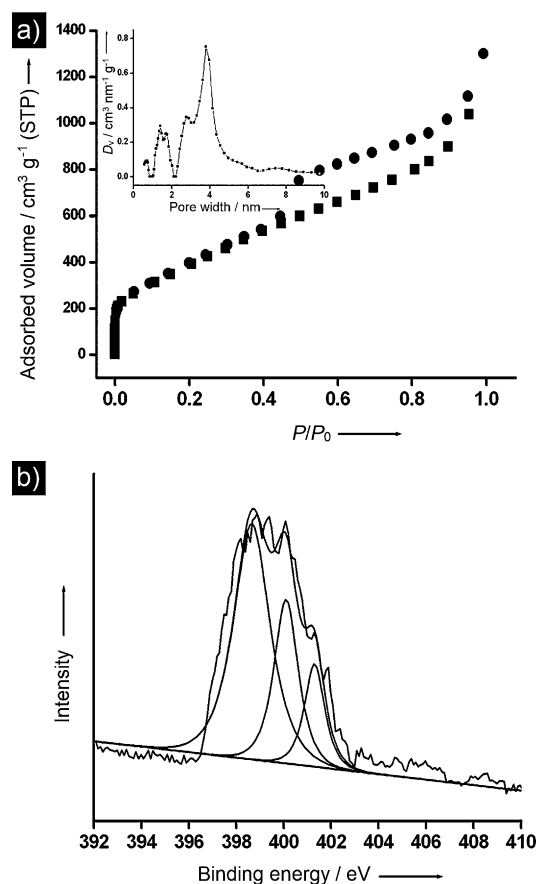


**Figure 3.** a) Nitrogen adsorption–desorption isotherms (inset: pore size distribution), and b) high-resolution N 1s XPS spectra of ANPGs.

X-ray photoelectron spectroscopy (XPS) proved particularly useful to elucidate the evolution of nitrogen functionalities during pyrolysis and gain insight into the pathway of nitrogen doping. The nitrogen precursor, pyrrole, has a simple structure with only one type of nitrogen atom within a pentagonal ring (N-5). However, the structure of the resulting NG is rather complex, with various types of nitrogens. As shown in Figure 3b, the high-resolution N1s peak could be further deconvoluted into three different peaks, at binding energies of 398.9, 400.1, and 401.3 eV. These peaks correspond to pyridinic-N (N-6), pyrrolic-N (N-5), and graphitic-N (N-Q), respectively. Obviously, during the carbonization process nitrogen atoms within the pentagonal ring of polypyrrole are converted into two types of nitrogen (N-6 and N-Q). Such easily accessible nitrogen-containing species (N-6 and N-Q) have been found to be responsible for the improved electrochemical activity of nitrogen-doped carbon materials.<sup>[9,10]</sup>

The electrochemical performance of the ANPGs electrode was evaluated by using a half-cell with sodium metal. Figure 4a shows representative cyclic voltammetry (CV) curves of the ANPGs electrode in the range 0.01–3 V. The sharp reduction peak at 0.42 V during the cathodic process in the first cycle is likely due to electrolyte decomposition and the formation of a solid electrolyte interphase (SEI) layer, as compared to

the lithium and sodium system.<sup>[2b,c,9g]</sup> This peak disappeared during the subsequent discharge, which can be attributed to isolation of the anode from the electrolyte due to the dense SEI layer formed on the surface of the anode in the first discharge. In addition, a pair of redox peaks observed at lower potential (near 0 V), similar to lithium insertion in carbonaceous materials,<sup>[12]</sup> can be ascribed to insertion–extraction of sodium ions in the interlayer of the graphitic microcrystallites. Notably, the second and following CV curves almost overlap, indicating that the ANPGs electrode offers good stability towards sodium ion insertion–extraction.

Figure 4b shows the charge–discharge profiles of the ANPGs electrode. The first charge–discharge cycle reveals the initial discharge and charge capacities to be 1003.2 and 349.7 mAh g<sup>-1</sup>, respectively, at a current density of 50 mA g<sup>-1</sup>. The large irreversible capacity loss likely originates from electrolyte decomposition and the formation of the SEI layer, coinciding with the results from the CV observations. Further investigations to reduce the irreversible capacity loss, by using additives in the electrolytes<sup>[13]</sup> or modifying the surface of the carbon materials,<sup>[14]</sup> are ongoing. In subsequent cycles, the ANPGs electrode shows obvious sloping charge–discharge curves and an indistinct plateau below 0.1 V. Results reported earlier have confirmed that the sloping voltage profile can be

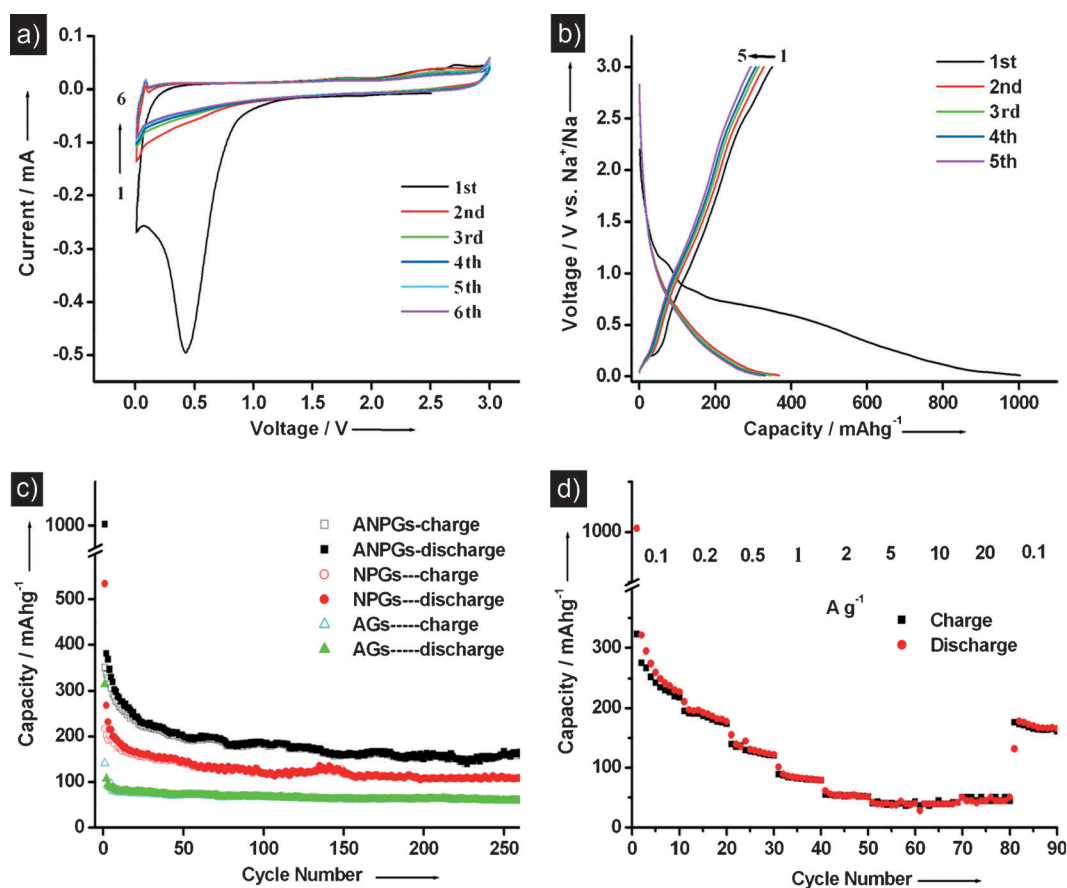


**Figure 4.** Electrochemical characterization and battery performance of the ANPGs as anode material for Na-ion batteries. a) CV curves of an ANPGs electrode between 0 and 3.0 V at a potential sweep rate of 0.1 mV s<sup>-1</sup>. b) Charge–discharge profiles of an ANPGs electrode at a current density of 50 mA g<sup>-1</sup>. c) Cycle performances of different electrodes at a current density of 50 mA g<sup>-1</sup>. d) Rate performance of an ANPGs electrode at different current densities.

attributed to the insertion of sodium between graphene layers, whilst sodium insertion into nanopores takes place at the lowest potentials.<sup>[2b,7a,15]</sup> Obviously, the majority of the capacity in our case originates from sodium insertion between graphene layers. Figure 4c compares the cycle performance of the ANPG, NPG, and AG electrodes at a current density of  $50 \text{ mA g}^{-1}$ . The ANPGs electrode shows an enhanced cycling performance compared to its NPG and AG counterparts. Specifically, the electrode retains a reversible capacity of  $155.2 \text{ mAh g}^{-1}$  even after 260 cycles. Although the initial Coulombic efficiency was very low, it increased dramatically upon cycling, reaching over 93% after 5 cycles and 98% after 20 cycles. Importantly, the ANPGs electrode still exhibits a good cyclic performance at a high current density of  $1 \text{ Ag}^{-1}$ , and the capacity still reaches  $80 \text{ mA g}^{-1}$  after 400 discharge and charge cycles (Figure S4). Our results are comparable to those achieved obtained by Tang et al.,<sup>[2b]</sup> and only few reports on NIB materials have achieved capacities of more than  $200 \text{ mAh g}^{-1}$ , at much lower current densities than reported here.<sup>[7a-c]</sup> Charge–discharge profiles and cycle performance recorded at a current density of  $50 \text{ mA g}^{-1}$  in the range 0.01–1.5 V are shown in Figure S5. A reversible capacity of over  $150 \text{ mAh g}^{-1}$  and more than 80% capacity retention after 200 cycles could be obtained at a much higher current density, which is more suitable for practical applications. To better understand the advantage of using ANPGs in NIBs, the rate performance of the ANPGs electrode was investigated (Figure 4d). The electrode delivered initial reversible capacities of 323.1, 194.8, 139.6, and  $88.9 \text{ mAh g}^{-1}$  at current rates of 0.1, 0.2, 0.5, and  $1 \text{ Ag}^{-1}$ , respectively. Interestingly, even at a very high current density of  $20 \text{ Ag}^{-1}$ , a reversible capacity of  $50 \text{ mAh g}^{-1}$  could be delivered. Thus, the electrode exhibits a high rate performance even at very fast sodium ions insertion–extraction speeds.

Based on the analyses above, the ANPGs electrode showed superior electrochemical performance. To the best of our knowledge, such high reversible capacity, good cycling performance, and high rate capability have seldom been achieved in previous reports on anode materials for NIBs.<sup>[2b-d]</sup> The improved electrochemical properties described herein can be explained by the unique 2D porous nanostructure and nitrogen doping, by analogy with lithium systems. The large surface area not only gives rise to the improved capacities owing to the pseudocapacitive effect, but also leads to a sufficiently large electrode/electrolyte interface to absorb sodium ions and promote rapid charge-transfer reactions.<sup>[8]</sup> Furthermore, the nitrogen doping in the ANPGs can enhance the electrochemical reactivity and electronic conductivity,<sup>[9,10]</sup> which makes an additional contribution to the exceptional performance. Most importantly, the 2D porous nanomaterials can offer shortened paths for sodium insertion/deinsertion, and the many pores may not only act as reservoirs for storage of sodium ions, but also accommodate the local volume change of the carbon anode material. TEM images of an ANPGs electrode after 50 cycles at a current density of  $50 \text{ mA g}^{-1}$  in the range 0.01–3 V are shown in Figure S6. In the presence of carbon black and binder, the 2D porous nanostructure could be mostly re-

tained, which confirms that the structure is stable in the repetitive sodium insertion and extraction process. Nonetheless, compared to the initial 2D porous nanostructures before cycling, there is a partial fracture, resulting in capacity fading.

Notwithstanding these advances, the development of NIBs is still at the early stages and the performance of NIBs still lags behind that of LIBs at this moment. The reaction mechanisms need to be carefully studied. In addition, not only new electrode materials but also solvents, sodium salts, current collectors, and other components should be thoroughly investigated, with an aim to reach optimal combinations for practical applications.<sup>[2d]</sup> With the further development of cathode materials,<sup>[2a,e,f]</sup> the sodium-ion full cell has attracted and will continue to attract great attention.<sup>[2d,i]</sup>

In summary, nitrogen-doped porous carbon sheets are successfully fabricated via chemical activation of PPy-functionalized graphene sheets with KOH. Unique compositional and structural features endow the nitrogen-doped porous carbon sheets with superior NIB performance, that is, a high reversible capacity ( $349.7 \text{ mAh g}^{-1}$  at a current density of  $50 \text{ mA g}^{-1}$ ), a good cycling stability (260 cycles), and a high rate capability ( $50 \text{ mAh g}^{-1}$  even at a very high current density of  $20 \text{ Ag}^{-1}$ ). The results demonstrate that the nitrogen-doped porous carbon sheets presented herein are a promising candidate for the construction of low-cost sodium ion battery systems that perform on a competitive level with Li-ion systems. Furthermore, we believe that the proposed synthesis strategy can be extended to other system, as the obtained ANPGs may find application in other fields, including lithium-ion batteries, supercapacitors, catalysis, and hydrogen storage.

## Experimental Section

**Synthesis of PPy-Functionalized GO Precursor:** The graphene oxide (GO) used in this work was prepared by a modified Hummers method.<sup>[16]</sup> A homogeneous graphene oxide suspension was prepared by dispersing 10 g GO solution ( $9.47 \text{ mg mL}^{-1}$ ) in 40 mL of  $\text{H}_2\text{O}$ . Then, cetyltrimethylammonium bromide (CTAB,  $(\text{C}_{16}\text{H}_{33})\text{N}(\text{CH}_3)_3\text{Br}$ , 0.73 g) was dissolved in the above solution in an ice bath. Ammonium persulfate (APS, 13.7 g) was added next. After magnetic stirring for 0.5 h and cooling to 0–5 °C, pyrrole monomer (0.83 mL) was added. The reaction was carried out at 0–5 °C during 24 h. A black precipitate was obtained and dried overnight at 80 °C in an oven.

**Synthesis of Activated PPy-Functionalized GSs:** Activated PPy-functionalized graphene sheets (ANPGs) were synthesized by chemical activation of PPy-functionalized GO precursor. 400 mg PPy-functionalized GO precursor was dispersed in 20 mL of 7 M KOH and stirred at room temperature for 24 h. The product was filtered and dried in an oven at 70 °C. Chemical activation was carried out for 2 h in a tubular furnace under a  $\text{N}_2$  gas flow at 800 °C (heating rate  $5^\circ\text{C min}^{-1}$ ). After activation the product was washed with an 8% HCl solution to neutralize KOH. The product was then frozen at  $-50^\circ\text{C}$  for 2 h and formed by freeze-drying of the ice solid under vacuum for 24 h. For comparison, a nitrogen-free sample (designated AG) was prepared by chemical activation of GO precursor, and PPy-functionalized GO precursor served as unactivated sample (designated NPG).



**Characterization:** The morphology and crystalline structure of as-obtained samples were characterized by using scanning electron microscopy (SEM, Hitachi S-4800) and transmission electron microscopy (TEM) recorded on a Tecnai G2 operating at 200 kV. X-ray diffraction (XRD) measurements were performed on a Bruker D8 Focus power X-ray diffractometer with  $\text{Cu}_{\text{K}\alpha}$  radiation. X-ray photoelectron spectroscopy (XPS) analysis was carried on an ESCALAB MK II X-ray instrument. Nitrogen adsorption and desorption isotherms were determined by nitrogen physisorption at 77 K on a Micromeritics ASAP 2020 analyzer. The pore size distribution was calculated via a nonlocal density functional theory method, using nitrogen adsorption data and assuming a slit pore mode.

**Electrochemistry:** The electrodes were prepared by mixing active material (80 wt%), acetylene black (10 wt%), and polyvinylidene fluoride (PVDF, 10 wt%) in *N*-methyl-2-pyrrolidone (NMP). After the slurries were uniformly spread onto a copper foil, the electrodes were dried at 80 °C in vacuum for 6 h. The electrodes were then pressed and cut into disks before transferring into an argon-filled glove box. Coin cells (CR2025) were assembled in the laboratory by using sodium metal as counter electrode, Celgard 2400 membrane as separator, and  $\text{NaPF}_6$  (1 M) in ethylene carbonate/dimethyl carbonate (EC/DMC, 1:1 w/w) as electrolyte. Galvanostatic charge-discharge tests were carried out on a Land Battery Measurement System (Land, PR China). Cyclic voltammetry (CV) and impedance measurements were performed by using a VMP3 Electrochemical Workstation (Bio-logic Inc.).

## Acknowledgements

This work was financially supported by the 100 Talents Programme of The Chinese Academy of Sciences, the Foundation for Innovative Research Groups of the National Natural Science Foundation of China (20921002), the National Natural Science Foundation of China (21101147), and the Jilin Province Science and Technology Development Program (20100102 and 20116008).

**Keywords:** batteries • carbon • doping • nanostructures • nitrogen

- [1] a) J. M. Tarascon, *Nat. Chem.* **2010**, *2*, 510; b) B. L. Ellis, W. R. M. Makahnouk, Y. Makimura, K. Toghill, L. F. Nazar, *Nat. Mater.* **2007**, *6*, 749–753; c) X. L. Wu, L. Y. Jiang, F. F. Cao, Y. G. Guo, L. J. Wan, *Adv. Mater.* **2009**, *21*, 2710–2714; d) Z. P. Song, T. Xu, M. L. Gordin, Y. B. Jiang, I. T. Bae, Q. F. Xiao, H. Zhan, J. Liu, D. H. Wang, *Nano Lett.* **2012**, *12*, 2205–2211; e) H. G. Jung, M. W. Jang, J. Hassoun, Y. K. Sun, B. Scrosati, *Nat. Commun.* **2011**, *2*, 516.
- [2] a) N. Yabuuchi, M. Kajiyama, J. Iwatate, H. Nishikawa, S. Hitomi, R. Okuyama, R. Usui, Y. Yamada, S. Komaba, *Nat. Mater.* **2012**, *11*, 512–517; b) K. Tang, L. J. Fu, R. J. White, L. H. Yu, M. M. Titirici, M. Antonietti, J. Maier, *Adv. Energy Mater.* **2012**, *2*, 873–877; c) Y. L. Cao, L. F. Xiao, M. L. Sushko, W. Wang, B. Schwenzer, J. Xiao, Z. M. Nie, L. V. Saraf, Z. G. Yang, J. Liu, *Nano Lett.* **2012**, *12*, 3783–3787; d) S. Komaba, W. Murata, T. Ishikawa, N. Yabuuchi, T. Ozeki, T. Nakayama, A. Ogata, K. Gotoh, K. Fujiwara, *Adv. Funct. Mater.* **2011**, *21*, 3859–3867; e) J. F. Qian, M. Zhou, Y. L. Cao, X. P. Ai, H. X. Yang, *Adv. Energy Mater.* **2012**, *2*, 410–414; f) Y. L. Cao, L. F. Xiao, W. Wang, D. Choi, Z. M. Nie, J. G. Yu, L. V. Saraf, Z. G. Yang, J. Liu, *Adv. Mater.* **2011**, *23*, 3155–3160; g) L. Zhao, J. M. Zhao, Y. S. Hu, H. Li, Z. B. Zhou, M. Armand, L. Q. Chen, *Adv. Energy Mater.* **2012**, *2*, 962–965; h) Y. Park, D. S. Shin, S. H. Woo, N. S. Choi, K. H. Shin, S. M. Oh, K. T. Lee, S. Y. Hong, *Adv. Mater.* **2012**, *24*, 3562–3567; i) A. Abouimrane, W. Weng, H. Eltayeb, Y. J. Cui, J. Niklas, O. Poluektov, K. Amine, *Energy Environ. Sci.* **2012**, *5*, 9632–9638.
- [3] J. Sangster, *J. Phase Equilib. Diffus.* **2007**, *28*, 571–579.
- [4] a) M. M. Doeff, Y. Ma, S. J. Visco, L. C. De Jonghe, *J. Electrochem. Soc.* **1993**, *140*, L169–L170; b) R. Alcántara, J. M. J. Mateos, J. L. Tirado, *J. Electrochem. Soc.* **2002**, *149*, A201–A205; c) E. Zhecheva, R. Stoyanova, J. M. Jiménez-Mateos, R. Alcántara, P. Lavela, J. L. Tirado, *Carbon* **2002**, *40*, 2301–2306.
- [5] R. Alcántara, J. M. Jiménez-Mateos, P. Lavela, J. L. Tirado, *Electrochem. Commun.* **2001**, *3*, 639–642.
- [6] P. Thomas, D. Billaud, *Electrochim. Acta* **2000**, *46*, 39–47.
- [7] a) D. A. Stevens, J. R. Dahn, *J. Electrochem. Soc.* **2000**, *147*, 1271–1273; b) R. Alcántara, P. Lavela, G. F. Ortiz, J. L. Tirado, *Electrochem. Solid-State Lett.* **2005**, *8*, A222–A225; c) P. Thomas, D. Billaud, *Electrochim. Acta* **2002**, *47*, 3303–3307; d) S. Wenzel, T. Hara, J. Janek, P. Adelhelm, *Energy Environ. Sci.* **2011**, *4*, 3342–3345.
- [8] a) J. H. Liu, X. W. Liu, *Adv. Mater.* **2012**, *24*, 4097–4111; b) X. Huang, X. Y. Qi, F. Boey, H. Zhang, *Chem. Soc. Rev.* **2012**, *41*, 666–686.
- [9] a) Z. S. Wu, W. Ren, L. Xu, F. Li, H. M. Cheng, *ACS Nano* **2011**, *5*, 5463–5471; b) F. Su, C. K. Poh, J. S. Chen, G. Xu, D. Wang, Q. Li, J. Lin, X. W. Lou, *Energy Environ. Sci.* **2011**, *4*, 717–724; c) L. Qie, W. M. Chen, Z. H. Wang, Q. G. Shao, X. Li, L. X. Yuan, X. L. Hu, W. X. Zhang, Y. H. Huang, *Adv. Mater.* **2012**, *24*, 2047–2050; d) H. Guo, Q. Gao, *J. Power Sources* **2009**, *186*, 551–556; e) L. F. Chen, X. D. Zhang, H. W. Liang, M. G. Kong, Q. F. Guan, P. Chen, Z. Y. Wu, S. H. Yu, *ACS Nano* **2012**, *6*, 7092–7102; f) Z. S. Wu, S. B. Yang, Y. Sun, K. Parvez, X. L. Feng, K. Mullen, *J. Am. Chem. Soc.* **2012**, *134*, 9082–9085; g) Y. Mao, H. Duan, B. Xu, L. Zhang, Y. S. Hu, C. C. Zhao, Z. X. Wang, L. Q. Chen, Y. S. Yang, *Energy Environ. Sci.* **2012**, *5*, 7950–7955.
- [10] a) Y. Q. Liu, D. C. Wei, Y. Wang, H. L. Zhang, L. P. Huang, G. Yu, *Nano Lett.* **2009**, *9*, 1752–1758; b) L. S. Panchookarla, K. S. Subrahmanyam, S. K. Saha, A. Govindaraj, H. R. Krishnamurthy, U. V. Waghmare, C. N. R. Rao, *Adv. Mater.* **2009**, *21*, 4726–4730; c) X. L. Li, H. L. Wang, J. T. Robinson, H. Sanchez, G. Diankov, H. J. Dai, *J. Am. Chem. Soc.* **2009**, *131*, 15939–15944; d) D. S. Geng, Y. Chen, Y. G. Chen, Y. L. Li, R. Y. Li, X. L. Sun, S. Y. Ye, S. Knights, *Energy Environ. Sci.* **2011**, *4*, 760–764; e) J. H. Li, Y. Wang, Y. Y. Shao, D. W. Matson, Y. H. Lin, *ACS Nano* **2010**, *4*, 1790–1798.
- [11] Y. W. Zhu, S. Murali, M. D. Stoller, K. J. Ganesh, W. W. Cai, P. J. Ferreira, A. Pirkle, R. M. Wallace, K. A. Cychosz, M. Thommes, D. Su, E. A. Stach, R. S. Ruoff, *Science* **2011**, *332*, 1537–1541.
- [12] K. Tang, R. J. White, X. K. Mu, M. M. Titirici, P. A. van Aken, J. Maier, *ChemSusChem* **2012**, *5*, 400–403.
- [13] a) S. K. Jeong, M. Inaba, R. Mogi, Y. Iriyama, T. Abe, Z. Ogumi, *Langmuir* **2001**, *17*, 8281–8286; b) Y. Hu, W. Kong, H. Li, X. Huang, L. Chen, *Electrochem. Commun.* **2004**, *6*, 126–131.
- [14] Z. S. Wu, L. L. Xue, W. C. Ren, F. Li, L. Wen, H. M. Cheng, *Adv. Funct. Mater.* **2012**, *22*, 3290–3297.
- [15] a) D. A. Stevens, J. R. Dahn, *J. Electrochem. Soc.* **2001**, *148*, A803–A811; b) P. Thomas, D. Billaud, *Electrochim. Acta* **2001**, *46*, 3359–3366.
- [16] a) W. S. Hummers, R. E. Offeman, *J. Am. Chem. Soc.* **1958**, *80*, 1339; b) D. C. Marcano, D. V. Kosynkin, J. M. Berlin, A. Sinitskii, Z. Z. Sun, A. Slesarev, L. B. Alemany, W. Lu, J. M. Tour, *ACS Nano* **2010**, *4*, 4806–4814.

Received: September 12, 2012

Revised: October 21, 2012

Published online on December 7, 2012